Long-Term Extreme Response Analysis of a Long-Span Pontoon Bridge

Finn-Idar Grøtta Giske[a,b,*], Knut Andreas Kvåle[c], Bernt Johan Leira[a], Ole Øiseth[c]

[a] *Department of Marine Technology, NTNU, 7491 Trondheim, Norway*
[b] *Multiconsult, Nedre Skøyen vei 2, 0213 Oslo, Norway*
[c] *Department of Structural Engineering, NTNU, 7491 Trondheim, Norway*

Abstract

For the assessment of extreme load effects needed in design of marine structures, a full long-term analysis is recognized as the most accurate approach. However, due to the very large number of structural response analyses traditionally needed for this approach, the computational effort is usually considered to increase above acceptable levels for complex structures such as floating bridges. In this paper, a framework for full long-term extreme response analysis is demonstrated for a long-span pontoon bridge subjected to wave loads. This framework utilizes some recently developed approaches which are based on the inverse first- and second-order reliability methods (IFORM and ISORM). Using the IFORM and ISORM approaches, characteristic values of the long-term extreme response are calculated in an efficient manner. By comparing with results obtained by full numerical integration, the accuracy of the methods is investigated. Particularly the ISORM method is seen to provide high accuracy. The full long-term analysis is also compared with the environmental contour method.

Keywords: marine structures, pontoon, floating bridge, extreme response, long-term response, IFORM, ISORM

1. Introduction

Fjord crossing technology is currently a research topic of high interest in Norway. Due to the width and depth of the fjords considered, floating bridges represent very relevant concepts as they utilize bouyancy for vertical support. The design of more extreme yet reliable fjord crossing structures motivates development of the methods for long-term stochastic extreme response analysis.

For the evaluation of extreme response of marine structures due to environmental loads, a full long-term analysis is recognized as the most accurate

*Corresponding author
Email address: finn.i.giske@ntnu.no (Finn-Idar Grøtta Giske)

design approach [1]. In principle, the full long-term approach takes into account all possible combinations of environmental parameters. This means that for straightforward methods such as full numerical integration and crude Monte Carlo simulation, a very large number of short-term response calculations have to be conducted. For complex structures like floating bridges, each short-term calculation is usually very time consuming, and the full long-term approach is often considered infeasible.

As an alternative to performing full long-term analyses, the environmental contour method [2, 3] is a widely used simplified approach. First, environmental contours corresponding to specified annual exceedance probabilities are determined without any consideration of the structural response. Traditionally the contours are determined using an inverse first-order reliability method (IFORM) approach [4], but alternative methods do exist [5, 6, 7]. The most critical point along the contour is then determined, and an estimate for the long-term extreme response is finally obtained. Only a few short-term response calculations are used, making the environmental contour method highly efficient. However, some sort of calibration against full long-term analysis is required [1]. Also, due to simplified modelling of response variability, the environmental contour method may perform poorly for certain types of structures [8, 9].

In recent years, efforts have been made to reduce the number of short-term calculations required for full long-term extreme response evaluation. These are based on the observation that many combinations of environmental parameters contribute little or nothing to the long-term extreme response. A copula based environmental modelling approach is proposed in [10], and the copula concept is further utilized in an adaptive refinement algorithm for more efficient long-term integration. In [11] an IFORM approach [4] is used to provide an estimate of the long-term extreme response. The IFORM method also indicates where the largest contribution to the long-term response is located, and this information is used in an importance sampling Monte Carlo simulation approach, improving the accuracy of the extreme response estimate. Further investigation of IFORM as a method for long-term extreme response estimation is carried out in [12], and in [13] an inverse second-order reliability method (ISORM) approach is proposed. These developments provide methods for carrying out full long-term analyses with a limited amount of short-term response calculations.

IFORM and ISORM are efficient and easily implemented methods, which is important for their practical application to long-term extreme response analysis. Still, it should be noted that having the long-term extreme response analysis formulated in terms of a reliability problem, as described in [12], a variety of methods from the field of structural reliability can also be applied. In particular, efficient simulation methods such as importance sampling [14, 15] and subset simulation [16, 17] could be used iteratively to calculate characteristic response values. Alternatively, efficient methods for reliability-based design optimization (RBDO), e.g. [18], could be used for direct calculation.

The long-term analysis can also be made more efficient by improving the efficiency of each short-term response calculation. One example is the method described in [19], which is demonstrated in [20] for pontoon bridges.

In the present paper it is shown how these recent developments can be used to perform full long-term extreme response analyses for a pontoon floating bridge subjected to first-order wave loads. Specifically, the inverse reliability approaches IFORM and ISORM [12, 13] are applied. It is demonstrated that the efficiency of these methods make full long-term extreme response analyses feasible, also for complex structures such as floating bridges. Furthermore, the framework proposed in this paper can be used for calibration of the environmental contour method.

2. Modelling the stochastic dynamic response of pontoon bridges

2.1. Stochastic modelling of waves

For a short-term period of duration $\tilde{T}$, the sea elevation is modelled as a homogeneous and stationary stochastic process with zero mean. The sea elevation process is denoted $\eta(x, y, t)$, where x, y are the spatial variables and t is the time variable. Assuming linear wave theory, the wave number $\kappa(\omega)$ is a function of angular frequency defined by the dispersion relation $\omega^2 = \kappa g \tanh(\kappa d)$, and the cross-spectral density between the wave elevation at two points (x_m, y_m) and (x_n, y_n) can be expressed in terms of a one-dimensional wave spectrum $S_\eta(\omega)$ and a spreading function $\Psi(\theta, \omega)$ as

$$S_{mn}(\omega) = S_\eta(\omega) \int_{-\pi}^{\pi} \Psi(\theta, \omega)\, e^{-i\kappa(\omega)(\Delta x \cos\theta + \Delta y \sin\theta)} d\theta.$$

Here $\Delta x = x_m - x_n$ and $\Delta y = y_m - y_n$ are the spatial separations of the points. For details we refer to [19].

The sea elevation is further assumed to be a Gaussian process which means that the cross-spectral densities provide a complete description of the process. Hence the wave situation is completely described by the wave spectrum $S_\eta(\omega)$ and the spreading function $\Psi(\theta, \omega)$. Various theoretical models given in terms of environmental parameters exist in the literature [21, 22]. In this paper we use the generalized Pierson-Moskowitz spectrum [22] given by

$$S_\eta(\omega) = \frac{{H_s}^2 T_z}{8\pi^2} \left(\frac{\omega T_z}{2\pi}\right)^{-5} \exp\left\{-\frac{1}{\pi}\left(\frac{\omega T_z}{2\pi}\right)^{-4}\right\},$$

where H_s is the significant wave height and T_z is the zero-crossing period. The spreading function is of the *cos-2s* type, defined by a mean wave direction $\bar{\Theta}$ relative to the x-axis and an ω-dependent spreading parameter $s(\omega)$ as

$$\Psi(\theta, \omega) = \frac{2^{2s(\omega)}\Gamma^2(s(\omega)+1)}{2\pi\Gamma(2s(\omega)+1)} \left(\cos^2\frac{\theta - \bar{\Theta}}{2}\right)^{s(\omega)},$$

where $\Gamma(\cdot)$ is the gamma function. Figure 1 shows the wave spectrum $S_\eta(\omega)$ plotted in the nondimensional scale $\omega T_z/2\pi$, and the spreading function is shown for different values of $s(\omega)$. In this paper we have used a constant spreading $s(\omega) = 10$, but it could equally well be defined as ω-dependent.

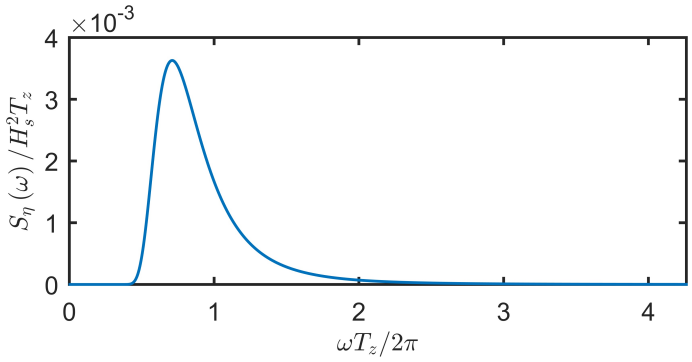

(a) The generalized Pierson-Moskowitz spectrum.

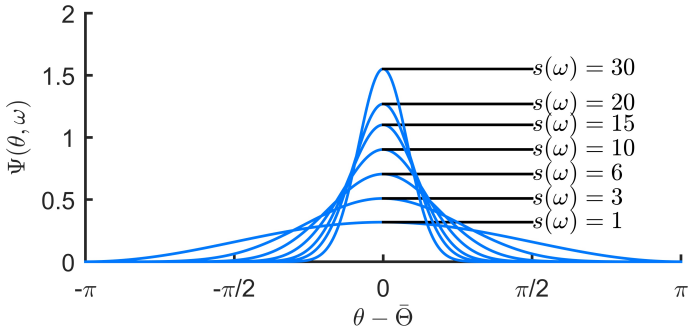

(b) The *cos-2s* spreading function.

Figure 1: Definition of the directional spectrum.

2.2. Stochastic modelling of first-order wave excitation loads

For pontoon floating bridges the structure will experience wave loads only where the pontoons are located. Considering the pontoons as rigid bodies, the bridge will experience loads in six degrees of freedom (DOFs) from each pontoon, three translational DOFs and three rotational DOFs. Thus, for a bridge with N pontoons we have loading in $6N$ DOFs, and we can define a wave excitation load vector $\boldsymbol{q}(t) = [\boldsymbol{q}_1(t), \boldsymbol{q}_2(t), \ldots, \boldsymbol{q}_N(t)]$, where $\boldsymbol{q}_m(t)$ denotes the 6-element load vector of pontoon number m. The individual components of the load vector $\boldsymbol{q}(t)$ can be denoted by $q_\mu(t)$, assigning a global index $\mu \in \{1, 2, \ldots, 6N\}$ to each DOF.

Consider pontoon m with a local coordinate system $(\tilde{x}, \tilde{y})$, which is located with its origin at the point (x_m, y_m) and rotated counterclockwise with an angle α_m relative to the global coordinate system (x, y) as shown in Fig. 2. The wave excitation loads due to a regular wave with angular frequency ω in the direction $\tilde{\beta}$ relative to the $\tilde{x}$-axis of the pontoon can be computed using linear potential theory software such as Wadam [23]. The loads are then reported in terms

of the 6-element complex transfer function vector $\boldsymbol{f}_m(\tilde{\beta},\omega)$. Considering only first-order wave loads, the wave excitation load process $\boldsymbol{q}_m(t)$ corresponding to the wave elevation process $\eta(x,y,t)$ can be obtained by superposition of loads from regular waves. This results in a stationary Gaussian load process $\boldsymbol{q}(t)$ with zero mean and a $6N$-by-$6N$ cross-spectral density matrix $\boldsymbol{S}_{\boldsymbol{q}}(\omega)$ whose elements are given by

$$S_{q_\mu q_\nu}(\omega) = S_\eta(\omega) \int_{-\pi}^{\pi} \Psi(\theta,\omega) f_\mu(\theta-\alpha_m,\omega)\overline{f_\nu(\theta-\alpha_n,\omega)} e^{-i\kappa(\omega)(\Delta x\cos\theta+\Delta y\sin\theta)} d\theta, \tag{1}$$

where the overline denotes complex conjugation. Here $f_\mu(\tilde{\beta},\omega)$ is the μ-th component of the total transfer function vector $\boldsymbol{f}(\tilde{\beta},\omega) = [\boldsymbol{f}_1(\tilde{\beta},\omega), \boldsymbol{f}_2(\tilde{\beta},\omega), \cdots, \boldsymbol{f}_N(\tilde{\beta},\omega)]$, i.e. the complex transfer function of the DOF μ.

A method for efficient calculation of the cross-spectral density matrix $\boldsymbol{S}_{\boldsymbol{q}}(\omega)$ based on the expression Eqn. (1) is given in [19, 20]. In [19] the derivation of the cross-spectral densities is also explained in more detail.

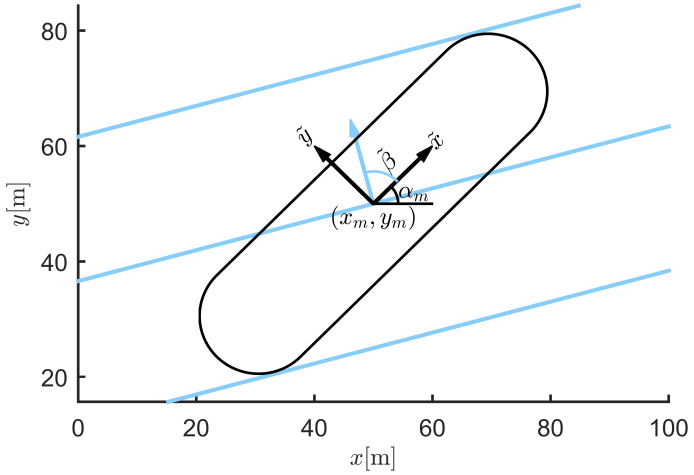

Figure 2: The local coordinate system of a pontoon.

2.3. Equations of motion

By employing the framework of the finite element method (FEM), the equations of motion describing the linear behaviour of a floating bridge can be written as

$$\boldsymbol{M}_s\ddot{\boldsymbol{u}}(t) + \boldsymbol{C}_s\dot{\boldsymbol{u}}(t) + \boldsymbol{K}_s\boldsymbol{u}(t) = \boldsymbol{q}_h(t),$$

where $\boldsymbol{M}_s$, $\boldsymbol{C}_s$ and $\boldsymbol{K}_s$ are the *structural* system matrices, excluding all fluid-structure interaction contributions; $\boldsymbol{u}(t)$ is the displacement vector; $\boldsymbol{q}_h(t)$ is the total hydrodynamic action, including both wave excitation and fluid-structure

interaction contributions; t is the time variable; and $\dot{\boldsymbol{u}} \equiv \frac{\partial \boldsymbol{u}}{\partial t}$. The total hydrodynamic action may be decomposed as follows:

$$\boldsymbol{q}_h(t) = -\left(\int_{-\infty}^{\infty} \boldsymbol{M}_h(t-\tau)\ddot{\boldsymbol{u}}(t)d\tau + \int_{-\infty}^{\infty} \boldsymbol{C}_h(t-\tau)\dot{\boldsymbol{u}}(t)d\tau + \boldsymbol{K}_h\boldsymbol{u}(t) \right) + \boldsymbol{q}(t).$$

Here the first term represents the fluid-structure interaction, with $\boldsymbol{M}_h(t)$ and $\boldsymbol{C}_h(t)$ being the time-domain representations of added mass and added damping respectively, and $\boldsymbol{K}_h$ being the hydrostatic stiffness. The second term, $\boldsymbol{q}(t)$, is the wave excitation load. Convolution integrals in the time domain are equivalent to multiplication in the frequency domain, such that the total hydrodynamic action may be written as follows by enforcing frequency domain notation:

$$\hat{\boldsymbol{q}}_h(\omega) = -\left(-\omega^2 \hat{\boldsymbol{M}}_h(\omega) + i\omega \hat{\boldsymbol{C}}_h(\omega) + \boldsymbol{K}_h \right) \hat{\boldsymbol{u}}(\omega) + \hat{\boldsymbol{q}}(\omega).$$

Here hats denote the frequency domain counterparts of the different quantities. Finally, the equation of motion of the system may be written on the following compact form, in the frequency domain:

$$\left(-\omega^2 \boldsymbol{M}(\omega) + i\omega \boldsymbol{C}(\omega) + \boldsymbol{K} \right) \hat{\boldsymbol{u}}(\omega) = \hat{\boldsymbol{q}}(\omega)$$

where $\boldsymbol{M}(\omega) = \boldsymbol{M}_s + \hat{\boldsymbol{M}}_h(\omega)$, $\boldsymbol{C}(\omega) = \boldsymbol{C}_s + \hat{\boldsymbol{C}}_h(\omega)$ and $\boldsymbol{K} = \boldsymbol{K}_s + \boldsymbol{K}_h$.

The second-order probabilistic properties of zero-mean response and wave excitation processes are fully described by cross-spectral densities. The stochastic frequency domain problem is easily solved by applying the power spectral density method. The cross-spectral density matrix of the response is then calculated as

$$\boldsymbol{S}_{\boldsymbol{u}}(\omega) = \boldsymbol{H}(\omega)\boldsymbol{S}_{\boldsymbol{q}}(\omega)\boldsymbol{H}(\omega)^H, \tag{2}$$

where $\boldsymbol{H}(\omega) = \left(-\omega^2 \boldsymbol{M}(\omega) + i\omega \boldsymbol{C}(\omega) + \boldsymbol{K} \right)^{-1}$ and $[\cdot]^H$ denotes the conjugate transpose. The cross-spectral density matrix $\boldsymbol{S}_{\boldsymbol{q}}(\omega)$ of the wave excitation load is found as explained in Section 2.2. More details on the subject may be found in e.g. [1, 24, 25, 26, 27].

3. Short-term response model for the case study bridge

The case study bridge consists of an S-shaped continuous girder box, which is supported on 20 pontoons. Figure 3 depicts the most important geometrical properties of the bridge. 16 symmetrically positioned cables provide side-support by fixation to the sea bed, cf. Fig. 4. The cross section of the girder is illustrated in Fig. 5. It is highlighted that the modelled bridge is considered merely as a useful example for the application of the methodology, and does not necessarily represent a feasible design.

3.1. Numerical response model set-up

The study carried out is performed using the approach presented in [27], and the reader is referred to that paper for a detailed description of the methodology for the numerical model set-up. The most important details are repeated here, for the convenience of the reader.

Two different sub-structures are used to create the full bridge model:

(I) A structural sub-structure, based on an Abaqus model incorporating all structural components and also including pontoon inertia and buoyancy.

(II) A hydrodynamic sub-structure, based on a Wadam model providing fluid-structure interaction terms, but excluding the buoyancy and pontoon inertia which are both included in (I).

To combine the two sub-structures, a modal decomposition is carried out in Abaqus [28]. The resulting mode shapes are referred to as the *dry* mode shapes, and are used as a new coordinate basis. The mode shapes are defined by the DOFs characterizing the rigid body motion of all pontoons. The frequency-dependent mass and damping contributions originating from the hydrodynamic model (II) are transformed to the coordinate basis defined by the dry mode shapes, before they are added to the modal system matrices from the structural model (I). It is noted that the results from the single pontoon analysis is duplicated and used for all pontoons, but necessary transformations and matrix book keeping are applied such that the orientation and additions are correct. The wave excitation cross-spectral density matrix $\boldsymbol{S_q}(\omega)$, given by Eqn. (1), is transformed to the coordinate basis given by the dry mode shapes, before the power spectral density method, cf. Eqn (2), is applied to calculate the spectral density of the response. In the final step, the response spectral density is transformed back to the physical DOFs of the pontoons. The main reason for carrying out this basis transformation is to avoid the extraction of all the free DOFs of the finite element model, as static condensation is not appropriate for dynamic problems. It should be noted that although a reduced order model is obtained, this is not a mode by mode approach because the modes will be coupled due to the hydrodynamic contributions.

3.2. Structural model

The continuous girder box is modelled in Abaqus with beam elements, with a generalized cross section characterized by the parameters shown in Tab. 1. The cables are modelled as beam elements, with circular cross sections.

In an initial static step, pre-tensioning of cables, cable bouyancy, global gravity, and static uplift forces are applied to the structure. The cables are pre-tensioned by assuming a constant negative temperature, which corresponds to a pre-tension of approximately 5000 kN. Fluid inertial effects are included for the cables; however, no drag damping is considered.

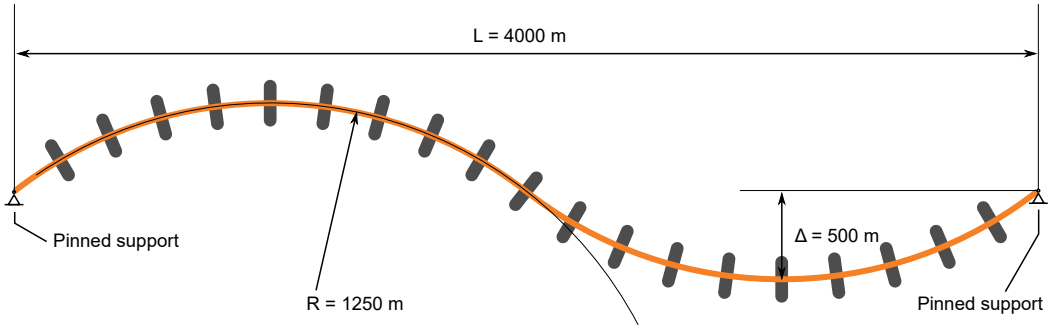

(a) Top view of main geometry.

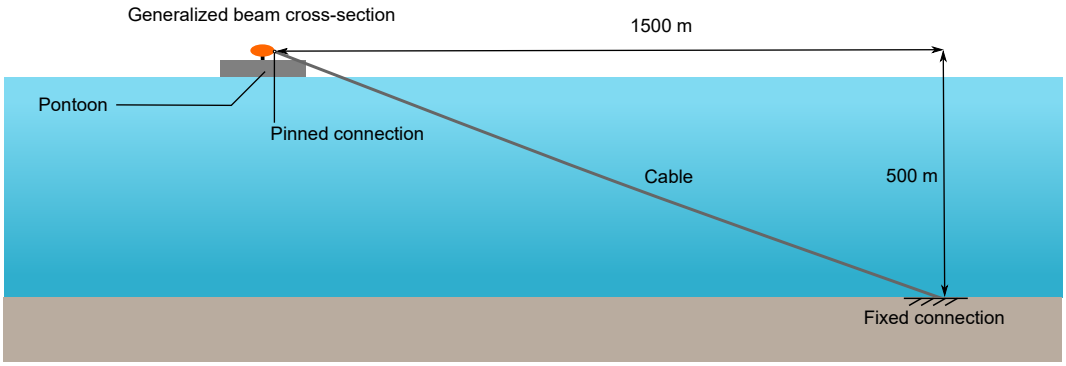

(b) Cable geometry.

Figure 3: Geometry of the bridge model.

Table 1: Parameters used for the generalized cross section.

Parameter	Value	Description
A	1.026 m^2	Cross-sectional area
I_y	10.79 m^4	Second moment of area about axis y
I_z	29.34 m^4	Second moment of area about axis z
J	24.92 m^4	Polar moment of area
z_c	3736 mm	Distance from bottom to neutral axis
y_c	0 mm	Distance from center to neutral axis

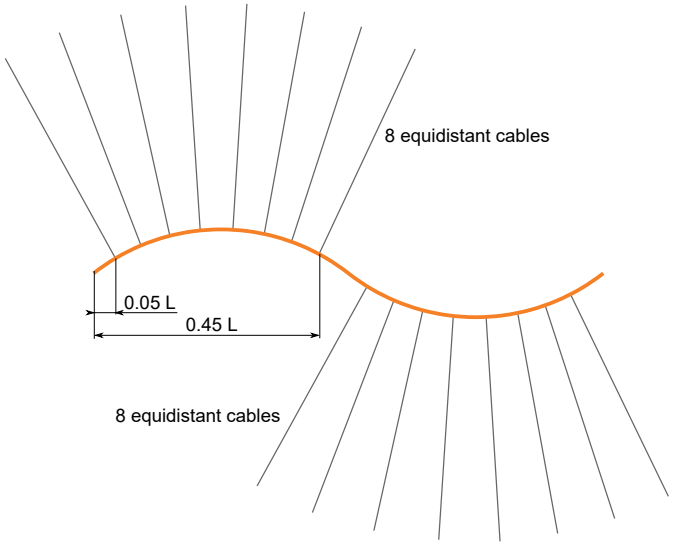

Figure 4: Position of cables. L refers to the horizontal distance, as defined in Fig. 3.

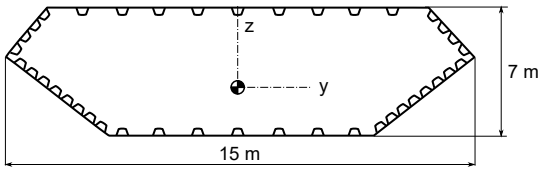

Figure 5: Main dimensions of cross section.

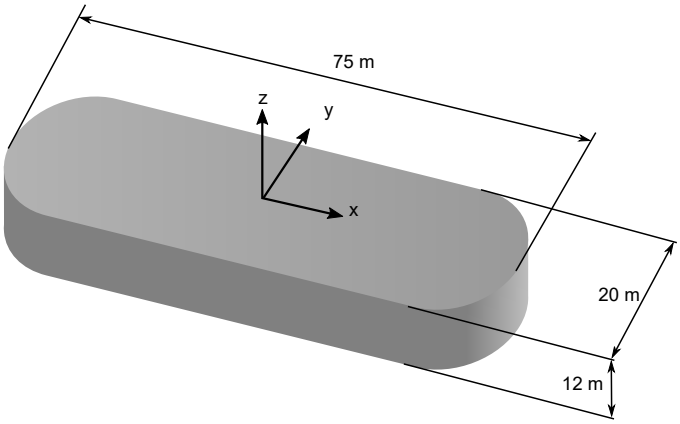

Figure 6: Main dimensions of pontoon and local coordinate system.

Table 2: Modal parameters from the numerical eigenvalue solution, corresponding to mode shapes illustrated in Fig. 7. The undamped natural frequency is denoted ω_n, and ξ is the corresponding critical damping ratio.

Mode number	ω_n [rad/s]	ξ [%]
Mode 1 (Fig. 7a)	0.11	1.53
Mode 2 (Fig. 7b)	0.15	1.28
Mode 3 (Fig. 7c)	0.16	1.18
Mode 4 (Fig. 7d)	0.18	1.02
Mode 5 (Fig. 7e)	0.20	0.88
Mode 6 (Fig. 7f)	0.24	0.79
Mode 7 (Fig. 7g)	0.28	0.75
Mode 8 (Fig. 7h)	0.33	0.81
Mode 9 (Fig. 7i)	0.38	1.06
Mode 10 (Fig. 7j)	0.45	1.87

3.3. Hydrodynamic pontoon model

A single hydrodynamic analysis, carried out in Wadam, is used to establish all system matrix contributions from the fluid-structure interaction. The geometry of the pontoon is depicted in Fig. 6. In the model set-up, buoyancy and inertia of the pontoon itself were added as local contributions to the bridge at the locations of the pontoons. The added hydrodynamic mass and damping coefficients, referring to the local coordinate system of the pontoon, are plotted in Figs. 8 and 9.

3.4. Modal parameters and shapes

Due to the frequency dependency of the hydrodynamic contributions, the eigenvalue problem is solved by iteration, as described in [27]. The resulting 10 first undamped natural frequencies and critical damping ratios are shown in Tab. 2, and the real part of the corresponding mode shapes are depicted in Fig. 7. Figure 7 reveals that the first 10 modes all have lateral motion patterns. From frequencies above the natural frequency of mode 10 and up, numerous cable modes are present.

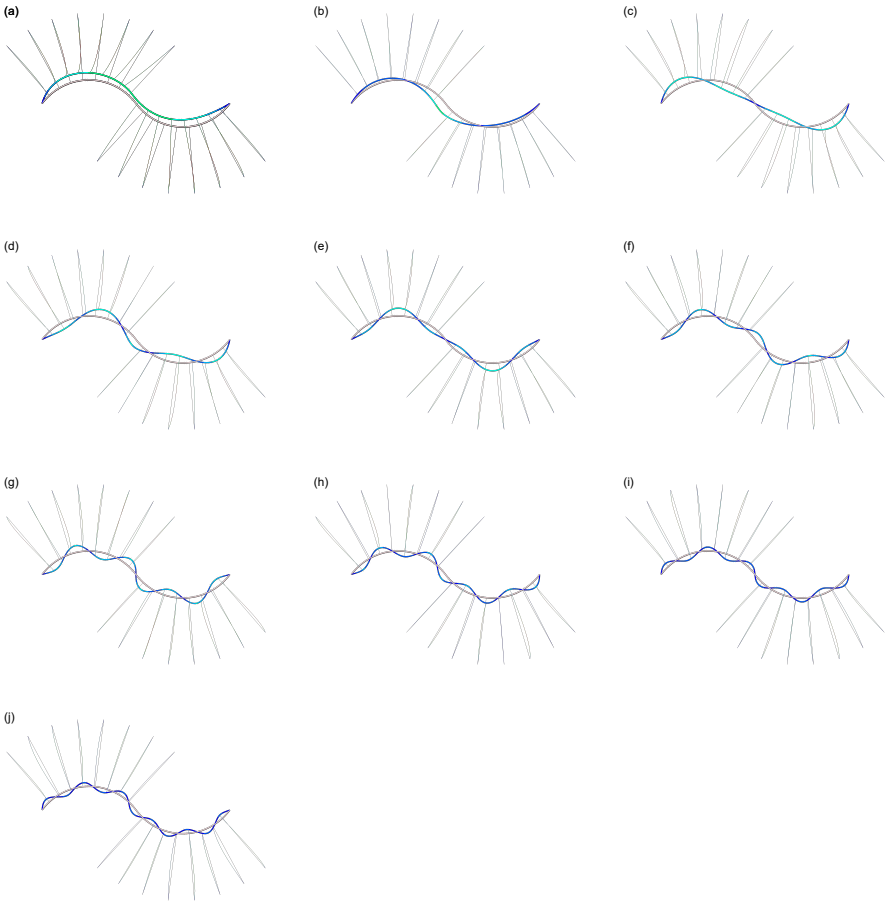

Figure 7: Mode shapes from numerical eigenvalue solution, corresponding to natural frequencies and damping ratios presented in Tab. 2. Note that the eigenvectors are complex, and their mode shape representation is therefore a snapshot. (a) Mode 1; (b) mode 2; (c) mode 3; (d) mode 4; (e) mode 5; (f) mode 6; (g) mode 7; (h) mode 8; (i) mode 9; (j) mode 10.

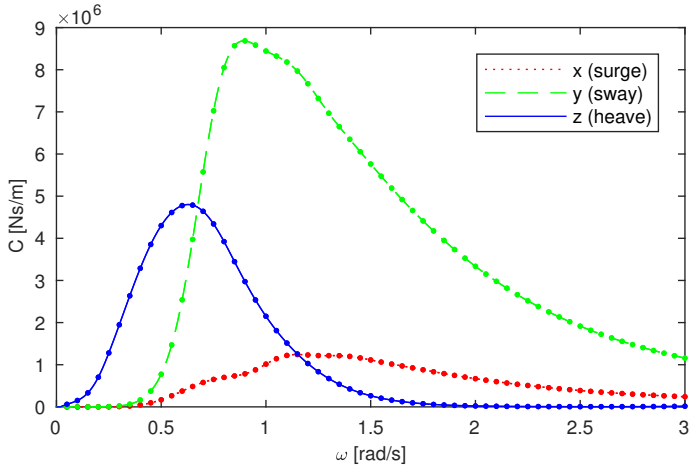

(a)

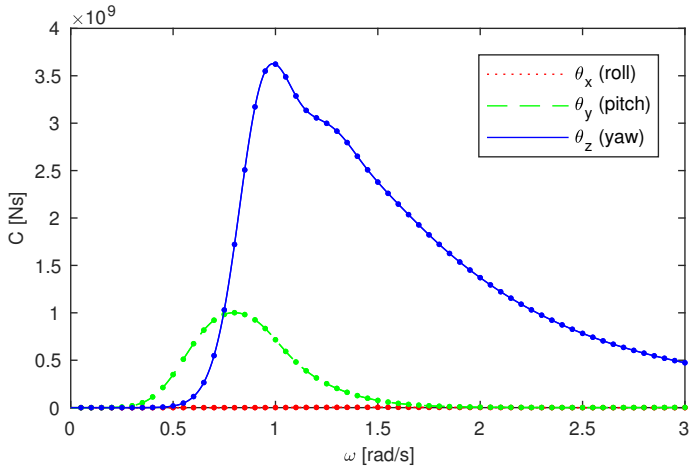

(b)

Figure 8: Translational (a) and rotational (b) damping coefficients of a single pontoon. Dots indicate the original data from Wadam, whilst lines represent interpolated data. The coordinates refer to the local coordinate system of the pontoon, as shown in Fig. 6.

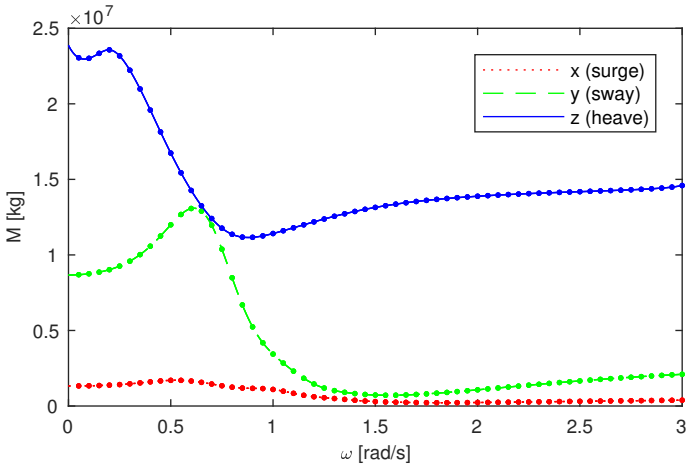

(a)

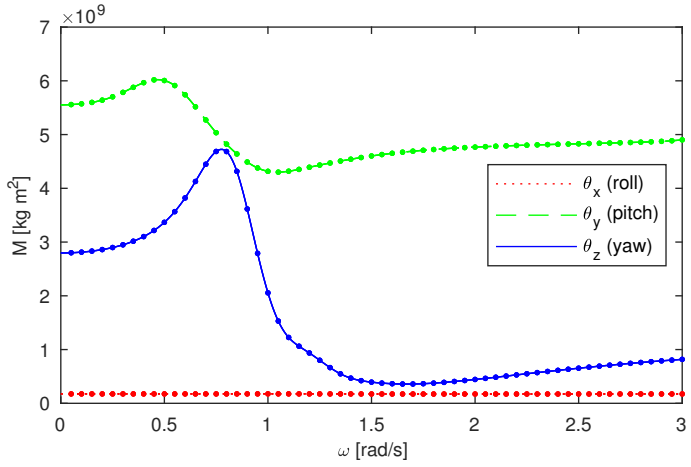

(b)

Figure 9: Translational (a) and rotational (b) mass coefficients of a single pontoon. Dots indicate the original data from Wadam, whilst lines represent interpolated data. The coordinates refer to the local coordinate system of the pontoon, as shown in Fig. 6.

4. Long-term extreme response

For the modelling of long-term extreme response of marine structures, the long-term situation can be considered as a collection of $\tilde{N}$ short-term states, each of duration $\tilde{T}$. During each short-term state the environmental processes are assumed stationary and defined by a set of n environmental parameters $\boldsymbol{W} = [W_1, W_2, \ldots, W_n]$. In this paper, we only consider the sea elevation, which is defined in terms of the environmental parameters $\boldsymbol{W} = [H_s, T_z, \bar{\Theta}]$, cf. Section 2.1. We will assume that the joint probability density function (PDF) of the environmental parameters, denoted $f_{\boldsymbol{W}}(\boldsymbol{w})$, is given. This PDF can be estimated by fitting a probabilistic model to a scatter diagram of recorded sea states [1].

The methodology presented in this paper for the calculation of extreme response is illustrated for a single response process. Specifically, we consider the horizontal transverse displacement of pontoon number five from the left in Fig. 3. This is the displacement along the local $\tilde{x}$-axis of this pontoon (see Fig. 2), and will henceforth simply be referred to as the response process, denoted $R(t)$. Being the response of a linear and time-invariant dynamical system, $R(t)$ will be a stationary Gaussian process with zero mean because the load process is. Hence, the response $R(t)$ is fully characterized by its spectral density $S_R(\omega)$, which is obtained as a diagonal element of the cross-spectral density matrix $\boldsymbol{S_u}(\omega)$ given by Eqn. (2). Figure 10 shows an example of the response spectrum $S_R(\omega)$ for a short-term situation where the environmental variables are given by $\boldsymbol{W} = [H_s, T_z, \bar{\Theta}] = [1\text{ m}, 6\text{ s}, -\pi/2]$.

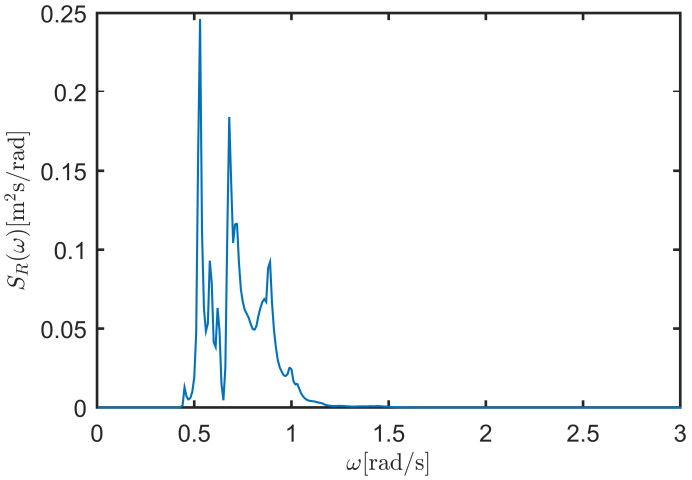

Figure 10: The response spectrum $S_R(\omega)$ when $\boldsymbol{W} = [H_s, T_z, \bar{\Theta}] = [1\text{ m}, 6\text{ s}, -\pi/2]$.

4.1. Short-term extreme value distribution

The maximal value of the response process $R(t)$ during a short-term period with given environmental variables $\boldsymbol{W}$ will be a random variable. This

short-term extreme response is denoted by $\tilde{R}|\boldsymbol{W}$ and its cumulative distribution function (CDF) is $F_{\tilde{R}|\boldsymbol{W}}(r|\boldsymbol{w}) = \text{Prob}[\tilde{R} \leq r|\boldsymbol{W} = \boldsymbol{w}] = \text{Prob}[\tilde{R} \leq r|H_s = h_s, T_z = t_z, \bar{\Theta} = \bar{\theta}]$. As explained in detail in [1], the short-term extreme value distribution $F_{\tilde{R}|\boldsymbol{W}}(r|\boldsymbol{w})$ can be found by assuming independent upcrossings of high levels r as

$$F_{\tilde{R}|\boldsymbol{W}}(r|\boldsymbol{w}) = \exp\left\{-\frac{\tilde{T}}{2\pi}\sqrt{\frac{m_2(\boldsymbol{w})}{m_0(\boldsymbol{w})}}\exp\left\{-\frac{r^2}{2m_0(\boldsymbol{w})}\right\}\right\}, \tag{3}$$

which holds for reasonably large values of r. Here the i-th moment $m_i(\boldsymbol{w})$ of the response spectrum $S_R(\omega)$ is defined as

$$m_i(\boldsymbol{w}) = \int_0^\infty \omega^i S_R(\omega) d\omega.$$

Note that $S_R(\omega)$ is dependent on the environmental parameters $\boldsymbol{w}$, though not written explicitly.

It should be noted that although Eqn. (1) and thereby Eqn. (3) are based on the assumption of homogeneity, which may be questioned for floating bridge applications, the general method presented in this paper is readily used along with other ways of calculating the short-term CDF $F_{\tilde{R}|\boldsymbol{W}}(r|\boldsymbol{w})$. The only required assumption is that the response process can be approximated as stationary for some short-term period $\tilde{T}$.

4.2. Long-term extreme response models

The long-term CDF of the short-term extreme value is denoted $F_{\tilde{R}}(r)$, and gives the distribution of the largest response value $\tilde{R}$ during an arbitrarily chosen short-term condition. This can be obtained as an average of all short-term CDFs $F_{\tilde{R}|\boldsymbol{W}}(r|\boldsymbol{w})$ weighted by the distribution $f_{\boldsymbol{W}}(\boldsymbol{w})$ of the environmental parameters. In order to estimate $f_{\boldsymbol{W}}(\boldsymbol{w})$ in the first place, an ergodicity assumption is required for the environmental parameters [29], and hence $F_{\tilde{R}}(r)$ should be expressed as an ergodic average [1, 29]. This yields the long-term extreme response formulation

$$F_{\tilde{R}}(r) = \exp\left\{\int_{\boldsymbol{w}}\left(\ln F_{\tilde{R}|\boldsymbol{W}}(r|\boldsymbol{w})\right) f_{\boldsymbol{W}}(\boldsymbol{w})\, d\boldsymbol{w}\right\}. \tag{4}$$

A very common approximate formulation, is given by the population mean

$$F_{\tilde{R}}(r) \approx \int_{\boldsymbol{w}} F_{\tilde{R}|\boldsymbol{W}}(r|\boldsymbol{w}) f_{\boldsymbol{W}}(\boldsymbol{w})\, d\boldsymbol{w}. \tag{5}$$

The formulations Eqns. (4) and (5) are discussed in more detail in [11, 12].

The long-term CDF $F_{\tilde{R}}(r)$ can be evaluated by solving the integrals in Eqns. (4) and (5) numerically. Unfortunately, full numerical integration requires a very large amount of short-term response calculations, since the short-term CDF $F_{\tilde{R}|\boldsymbol{W}}(r|\boldsymbol{w})$ must be calculated for a very large number of environmental conditions. This motivates the use of inverse reliability methods for calculation of long-term extreme response.

4.3. Writing the long-term CDF in terms of a reliability problem

In order to use reliability methods for evaluating the long-term CDF $F_{\tilde{R}}(r)$, it must be rewritten in terms of a reliability problem. A reliability problem in the general sense [30] is an integral of the form

$$\int\limits_{G(\boldsymbol{v})\leq 0} f_{\boldsymbol{V}}(\boldsymbol{v})d\boldsymbol{v},$$

where $\boldsymbol{V}$ is a random vector with joint PDF $f_{\boldsymbol{V}}(\boldsymbol{v})$ and $G(\boldsymbol{v})$ is a function referred to as the limit state function.

For the approximate formulation Eqn. (5), it is well known that the long-term CDF can be expressed in terms of a reliability problem by rewriting

$$\int\limits_{\boldsymbol{w}} F_{\tilde{R}|\boldsymbol{W}}\left(r|\boldsymbol{w}\right) f_{\boldsymbol{W}}\left(\boldsymbol{w}\right) d\boldsymbol{w} = \int\limits_{\boldsymbol{w}} \int\limits_{\tilde{r}\leq r} f_{\tilde{R}|\boldsymbol{W}}\left(\tilde{r}|\boldsymbol{w}\right) d\tilde{r} f_{\boldsymbol{W}}\left(\boldsymbol{w}\right) d\boldsymbol{w}.$$

Introducing the random vector $\bar{\boldsymbol{V}} = [\boldsymbol{W}, \tilde{R}]$, whose joint PDF is given by $f_{\bar{\boldsymbol{V}}}\left(\bar{\boldsymbol{v}}\right) = f_{\tilde{R}|\boldsymbol{W}}\left(\tilde{r}|\boldsymbol{w}\right) f_{\boldsymbol{W}}\left(\boldsymbol{w}\right)$, Eqn. (5) yields

$$F_{\tilde{R}}\left(r\right) \approx \int\limits_{\tilde{r}\leq r} f_{\bar{\boldsymbol{V}}}\left(\bar{\boldsymbol{v}}\right) d\bar{\boldsymbol{v}} = 1 - \int\limits_{r\leq \tilde{r}} f_{\bar{\boldsymbol{V}}}\left(\bar{\boldsymbol{v}}\right) d\bar{\boldsymbol{v}}.$$

Finally, we obtain

$$F_{\tilde{R}}\left(r\right) \approx 1 - \int\limits_{G_r(\bar{\boldsymbol{v}})\leq 0} f_{\bar{\boldsymbol{V}}}\left(\bar{\boldsymbol{v}}\right) d\bar{\boldsymbol{v}}, \tag{6}$$

where $G_r(\bar{\boldsymbol{v}}) = r - \tilde{r} = r - \bar{v}_{n+1}$, with $\bar{v}_{n+1}$ being the $(n+1)$-th component of the vector $\bar{\boldsymbol{v}}$.

The exact formulation Eqn. (4) can be used directly to obtain a better approximation for the long-term CDF in terms of a reliability problem [12, 13, 31]. Equation (4) is rewritten by multiplying and dividing the integral by some freely chosen constant $C \geq 1$. Then unity is added and subtracted, keeping in mind that $\int_{\boldsymbol{w}} f_{\boldsymbol{W}}\left(\boldsymbol{w}\right) d\boldsymbol{w} = 1$. Specifically, we obtain

$$F_{\tilde{R}}\left(r\right) = \exp\left\{-C\left(1 - \int_{\boldsymbol{w}} \left(1 + \frac{1}{C}\ln F_{\tilde{R}|\boldsymbol{W}}(r|\boldsymbol{w})\right) f_{\boldsymbol{W}}\left(\boldsymbol{w}\right) d\boldsymbol{w}\right)\right\}.$$

Introducing the random variable Y defined by the CDF $F_{Y|\boldsymbol{W}}(y|\boldsymbol{w}) = \max\left\{1 + \frac{1}{C}\ln F_{\tilde{R}|\boldsymbol{W}}(y|\boldsymbol{w}), 0\right\}$, the factor $1+\frac{1}{C}\ln F_{\tilde{R}|\boldsymbol{W}}(r|\boldsymbol{w})$ in the above integral can be replaced by $F_{Y|\boldsymbol{W}}(r|\boldsymbol{w})$. This yields the approximation

$$F_{\tilde{R}}\left(r\right) \approx \exp\left\{-C\left(1 - \int_{\boldsymbol{w}} F_{Y|\boldsymbol{W}}\left(r|\boldsymbol{w}\right) f_{\boldsymbol{W}}\left(\boldsymbol{w}\right) d\boldsymbol{w}\right)\right\}. \tag{7}$$

Here the domain where $1 + \frac{1}{C}\ln F_{\tilde{R}|\boldsymbol{W}}(r|\boldsymbol{w}) < 0$ is disregarded. This is a very good approximation for large values of r, since $F_{\tilde{R}|\boldsymbol{W}}(r|\boldsymbol{w})$ will be close to unity.

Furthermore, by increasing the value of C, the approximation will improve. Now the approximation Eqn. (7) obtained directly from the exact formulation Eqn. (4) can be written in terms of a reliability problem using the same approach as for the approximate formulation. Finally, the long-term CDF is expressed as

$$F_{\tilde{R}}(r) \approx \exp\left\{-C \int\limits_{G_r(\boldsymbol{v})\leq 0} f_{\boldsymbol{V}}(\boldsymbol{v})\, d\boldsymbol{v}\right\}, \tag{8}$$

where $\boldsymbol{V} = [\boldsymbol{W}, Y]$ and $G_r(\boldsymbol{v}) = r - y = r - v_{n+1}$.

4.4. Calculation of extreme response using inverse reliability methods

When long-term extreme responses are calculated for design purposes, we usually seek the characteristic response value r_q which has a specified annual exceedance probability q. This may also be referred to as the response value with a return period of $1/q$ years, or simply the $1/q$-year response. The characteristic response r_q is found by requiring

$$1 - F_{\tilde{R}}(r_q) = \frac{q}{\tilde{N}},$$

where $\tilde{N} = 1\ \mathrm{yr}/\tilde{T}$ is the number of short-term periods in one year. In this paper we have used $\tilde{T} = 3$ h, which gives $\tilde{N} = 365 \cdot 8 = 2920$. If we denote by $\tilde{r}_q$ the long-term extreme response obtained when using the approximate formulation Eqn. (5) for the long-term CDF, we have from Eqn. (6) that $\tilde{r}_q$ must satisfy

$$\int\limits_{G_{\tilde{r}_q}(\overline{\boldsymbol{v}})\leq 0} f_{\bar{\boldsymbol{V}}}(\overline{\boldsymbol{v}})\, d\overline{\boldsymbol{v}} = \frac{q}{\tilde{N}}. \tag{9}$$

Similarly, using Eqn. (8), which corresponds to the exact formulation Eqn. (4), yields the following equation for r_q:

$$\int\limits_{G_{r_q}(\boldsymbol{v})\leq 0} f_{\boldsymbol{V}}(\boldsymbol{v})\, d\boldsymbol{v} = -\frac{1}{C}\ln\left(1 - \frac{q}{\tilde{N}}\right). \tag{10}$$

Now the problem of finding $\tilde{r}_q$ and r_q that satisfies Eqns. (9) and (10) can be solved in an approximate manner using inverse reliability methods. Taking Eqn. (9) as an example, the random vector $\bar{\boldsymbol{V}}$ is transformed into a vector $\boldsymbol{U}$ of independent standard normal random variables by the Rosenblatt transformation $\boldsymbol{U} = T(\bar{\boldsymbol{V}})$, and Eqn. (9) becomes

$$\int\limits_{g_{\tilde{r}_q}(\boldsymbol{u})\leq 0} f_{\boldsymbol{U}}(\boldsymbol{u})\, d\boldsymbol{u} = \frac{q}{\tilde{N}}, \tag{11}$$

where $g_{\tilde{r}_q}(\boldsymbol{u}) = G_{\tilde{r}_q}(T^{-1}(\boldsymbol{u})) = \tilde{r}_q - \tilde{r}(\boldsymbol{u})$ is the transformed limit state function and $f_{\boldsymbol{U}}(\boldsymbol{u})$ is the multivariate standard normal PDF. Using the first-order reliability method (FORM) to approximate the integral in Eqn. (11), the inverse FORM (IFORM) problem can be derived as

$$\tilde{r}_q^{\mathrm{F}} = \max \tilde{r}(\boldsymbol{u}); \text{ subject to } |\boldsymbol{u}| = \beta, \tag{12}$$

where $\beta = -\Phi^{-1}(q/\tilde{N})$ with $\Phi(\cdot)$ being the standard normal CDF. Thus, solving the IFORM problem Eqn. (12) provides an estimate $\tilde{r}_q^{\mathrm{F}}$ for the characteristic extreme response value $\tilde{r}_q$. In this work we have used the solution algorithm proposed in [12]. For details on the transformation to standard normal variables and the derivation of the IFORM problem the reader is referred to [4, 12, 30].

If, on the other hand, the second-order reliability method (SORM) is used to approximate the integral in Eqn. (11), an inverse SORM (ISORM) method can be derived. In [13] an ISORM approach is proposed where the IFORM problem Eqn. (12) is solved repeatedly, updating the value of β which is unknown in this case. The characteristic extreme response estimate provided by the ISORM method is denoted $\tilde{r}_q^{\mathrm{S}}$.

The inverse reliability methods IFORM and ISORM can be applied to Eqn. (10) using the same approach as described above, providing long-term extreme response estimates that approximate r_q. We denote these estimates by r_q^{F} and r_q^{S} respectively. The only differences will be that $\boldsymbol{V}$ is transformed instead of $\bar{\boldsymbol{V}}$, and that $\beta = -\Phi^{-1}\left(-\frac{1}{C}\ln\left(1-\frac{q}{\tilde{N}}\right)\right)$.

It is reported in [12, 13] that the use of reliability methods appears to give good accuracy for the calculated long-term extreme response while keeping the number of required short-term response calculations within reasonable levels.

4.5. Environmental contour method

Even though IFORM and ISORM represent efficient methods for extreme response evaluation, some cases may still call for a more simplified approach. The environmental contour method has been proposed as such a simplified approach for estimating characteristic long-term extreme response values [3]. It is developed in [4] based on the approximate formulation Eqn. (5) and the IFORM approximation. In fact, the method can be considered as a special case of the IFORM problem Eqn. (12) where the short-term extreme response is regarded as deterministic [4].

The environmental contour corresponding to a given annual exceedance probability q is found from the joint environmental PDF $f_{\boldsymbol{W}}(\boldsymbol{w})$ without any consideration of the structural response. Then, the most unfavourable combination of environmental parameters along this q-probability contour, referred to as the design point, is identified. In this paper the design point, denoted by $\hat{\boldsymbol{w}}$, is taken as the point along the contour where the median, i.e. the 0.5-fractile, of the short-term distribution $F_{\tilde{R}|\boldsymbol{W}}(r|\boldsymbol{w})$ attains its maximal value. This maximization problem is the same as the IFORM problem Eqn. (12), but since the extreme response is regarded deterministic the dimension is reduced by one.

Nevertheless, the same solution algorithm can be applied to obtain the design point $\hat{\boldsymbol{w}}$. In order to account for the randomness of the short-term extreme value, the characteristic response value is chosen as the p-fractile, $p > 0.5$, of the short-term extreme value distribution $F_{\tilde{R}|\boldsymbol{W}}(r|\hat{\boldsymbol{w}})$ at the design point. The appropriate value for p must be validated by a full long-term analysis [1].

It is worth mentioning that it is possible to derive an environmental contour method based on the IFORM solution of the exact formulation Eqn. (4). In that case, we would use the short-term distribution $F_{Y|\boldsymbol{W}}(y|\boldsymbol{w})$ instead of $F_{\tilde{R}|\boldsymbol{W}}(r|\boldsymbol{w})$, and the q-probability contour would be defined in the standard normal space by a radius $\beta = -\Phi^{-1}\left(-\frac{1}{C}\ln\left(1-\frac{q}{\tilde{N}}\right)\right)$ instead of $\beta = -\Phi^{-1}(q/\tilde{N})$. This would, however, introduce contours dependent on the parameter C, and the appealing simplicity of the contour method would be undermined.

5. Numerical results

5.1. Environmental models

The environmental parameters defining the short-term wave situation according to Section 2.1 are the significant wave height H_s, the zero-crossing period T_z and the mean wave direction $\bar{\Theta}$. Using the conditional modelling approach described in [32, 33], the CDF of the significant wave height H_s is given by a 2-parameter Weibull distribution

$$F_{H_s}(h) = 1 - \exp\left\{-\left(\frac{h}{\alpha}\right)^{\beta}\right\}, \tag{13}$$

and the zero-crossing period T_z has a conditional lognormal distribution

$$F_{T_z|H_s}(t|h) = \Phi\left(\frac{\ln t - \mu(h)}{\sigma(h)}\right), \tag{14}$$

where $\mu(h) = a_0 + a_1 h^{a_2}$ and $\sigma(h) = b_0 + b_1 e^{b_2 h}$. Here α, β and $a_0, a_1, a_2, b_0, b_1, b_2$ are the parameters of the distributions. For the mean wave direction $\bar{\Theta}$, we use a distribution independent of H_s and T_z, given by the CDF

$$F_{\bar{\Theta}}(\theta) = \begin{cases} 0, & \text{for } \theta < -\pi, \\ 2\left(1+\frac{\theta}{\pi}\right)^2, & \text{for } -\pi \le \theta < -\frac{\pi}{2}, \\ 1-2\left(\frac{\theta}{\pi}\right)^2, & \text{for } -\frac{\pi}{2} \le \theta < 0, \\ 1, & \text{for } \theta \ge 0. \end{cases} \tag{15}$$

This means that the PDF $f_{\bar{\Theta}}(\theta)$, obtained by differentiating Eqn. (15) with respect to θ, is piecewise linear between $-\pi$ and 0 with a peak at $-\frac{\pi}{2}$. Similarly, the PDFs $f_{H_s}(h)$ and $f_{T_z|H_s}(t|h)$ can be obtained by differentiating Eqns. (13) and (14) with respect to h and t respectively, and the joint PDF of the environmental parameters is given as

$$f_{\boldsymbol{W}}(\boldsymbol{w}) = f_{H_s,T_z,\bar{\Theta}}(h,t,\theta) = f_{H_s}(h)\, f_{T_z|H_s}(t|h)\, f_{\bar{\Theta}}(\theta). \tag{16}$$

Table 3: Overview of the considered environmental models.

		H_s			T_z							$\bar{\Theta}$
Name	Joint PDF	Value/CDF	α	β	Value/CDF	a_0	a_1	a_2	b_0	b_1	b_2	Value/CDF
EM1	Eqn. (16)	Eqn. (13)	0.587	1.59	Eqn. (14)	0.151	0.339	0.167	0.07	0.3449	−0.6219	Eqn. (15)
EM2	Eqn. (17)	Eqn. (13)	”	”	$\exp\{\mu(H_s)\}$	”	”	”	n/a	n/a	n/a	Eqn. (15)
EM3	Eqn. (18)	Eqn. (13)	”	”	Eqn. (14)	”	”	”	0.07	0.3449	−0.6219	$-\pi/2$
EM4	Eqn. (18)	Eqn. (13)	0.550	1.53	Eqn. (14)	−0.120	1.439	0.150	0.07	0.0978	−0.0382	$-\pi/2$

The environmental model Eqn. (16) where all three environmental parameters are random variables will be referred to as EM1. Different environmental models can be obtained by considering some of the environmental parameters as deterministic. If for instance the zero-crossing period is taken as the conditional median obtained from the CDF Eqn. (14), i.e. $T_z = \exp\{\mu(H_s)\}$, we obtain the environmental model

$$f_{\boldsymbol{W}}(\boldsymbol{w}) = f_{H_s,\bar{\Theta}}(h,\theta) = f_{H_s}(h)\, f_{\bar{\Theta}}(\theta). \tag{17}$$

This will be referred to as EM2. We also consider an environmental model where the mean wave direction is given as $\bar{\Theta} = -\pi/2$. This yields

$$f_{\boldsymbol{W}}(\boldsymbol{w}) = f_{H_s,T_z}(h,t) = f_{H_s}(h)\, f_{T_z|H_s}(t|h)\,, \tag{18}$$

which will be referred to as EM3. The environmental models EM1, EM2 and EM3 will all have the same values for the distribution parameters. We also consider a model EM4, which is given by Eqn. (18) with different parameter values. An overview of the environmental models and their distribution parameters is provided in Tab. 3.

The environmental models are illustrated in Fig. 11 by displaying the environmental contours corresponding to annual exceedance probabilities $q = 10^{-2}$ and $q = 10^{-4}$, i.e. the 100-year and 10 000-year contours. For the two-dimensional models EM2, EM3 and EM4, the isoprobability contours obtained from the PDFs Eqns. (17) and (18) are also shown. Note that EM2 and EM3 are obtained from EM1 by regarding as deterministic T_z and $\bar{\Theta}$ respectively. EM4 represent a different model entirely. However, for all the models considered, the significant wave heights H_s with return periods of 100 and 10 000 years are approximately 2.9 m and 3.5 m respectively.

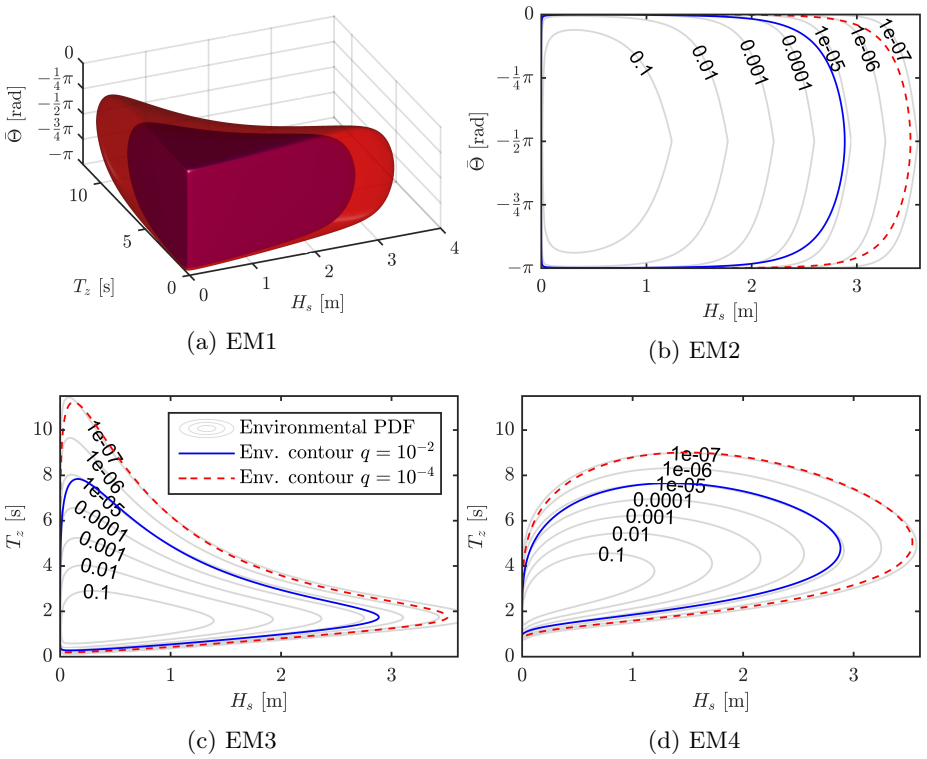

(a) EM1 (b) EM2

(c) EM3 (d) EM4

Figure 11: The contours corresponding to annual exceedance probabilities $q = 10^{-2}$ and $q = 10^{-4}$ for the different environmental models. For the two-dimensional models EM2, EM3 and EM4 the PDFs are illustrated by displaying the isoprobability contours. EM2 and EM3 are obtained from EM1 by regarding as deterministic T_z and $\bar{\Theta}$ respectively.

5.2. Characteristic extreme response values

5.2.1. Inverse reliability methods

Estimates for the characteristic response value r_q were calculated using the methods described in Section 4.4. The value $\tilde{r}_q$ was obtained by numerically solving the integral in the approximate formulation Eqn. (5), and $\tilde{r}_q^{\mathrm{F}}$ and $\tilde{r}_q^{\mathrm{S}}$ denote the IFORM and ISORM approximations of $\tilde{r}_q$. Similarly, r_q was found by applying numerical integration to the formulation Eqn. (4) and the reliability method approximations are denoted r_q^{F} and r_q^{S}. For r_q^{F} and r_q^{S}, different values of the constant C in Eqns. (8) and (10) could be used. In this paper, $C = 1$ is used for r_q^{F}, while the values $C = 1$, $C = 10^4$ and $C = 10^6$ are used for r_q^{S}.

For the calculation of $\tilde{r}_q$ and r_q by numerical integration, the ranges of the integration variables were $H_s \in [0, 10]$ m, $T_z \in [0.4, 20]$ s, and $\bar{\Theta} \in [-\pi, 0]$. The applied bin sizes were $\Delta H_s = 0.1$ m, $\Delta T_z = 0.2$ s, $\Delta\bar{\Theta} = \pi/39$ for EM1, $\Delta H_s = 0.05$ m, $\Delta\bar{\Theta} = \pi/39$ for EM2 and $\Delta H_s = 0.05$ m, $\Delta T_z = 0.05$ s for EM3 and EM4. It should be noted that these ranges and bin sizes are chosen such that $\tilde{r}_q$ and r_q can be regarded as exact values, and the number of integration points may therefore be excessive.

The obtained values for the characteristic extreme response estimates are presented in Tabs. 4 and 5 for annual exceedance probabilities $q = 10^{-2}$ and $q = 10^{-4}$, respectively. When compared to the values $\tilde{r}_q$ and r_q, it is seen that the reliability method approximations provide reasonable estimates for the characteristic response value. Especially the ISORM method with C chosen as 10^4 or 10^6 yields very good estimates.

In Tabs. 4 and 5, the characteristic response values are seen to vary quite a lot between the different environmental models. This is a result of the response being very sensitive to the zero-crossing period T_z. In Fig. 11 it is seen that large values of T_z have a larger probability of occurrence for EM4 than for EM3, resulting in a significantly larger extreme response. For EM2, T_z is fixed at its median value, disregarding large values of T_z. This results in a smaller extreme response for EM2. EM1 and EM3, on the other hand, have the same model for T_z and give quite similar results.

For each of the extreme response estimates in Tabs. 4 and 5, the corresponding number of executed short-term response calculations, denoted by n_{st} or similar, is reported in Tabs. 6 and 7. It is clear that IFORM and ISORM represent efficient methods for full long-term extreme response analysis. ISORM roughly doubles the computational effort compared to IFORM.

5.2.2. Environmental contour method

Using some common choices for the fractile level p, characteristic extreme response estimates denoted r_q^p were obtained for the environmental contour method. These estimates are presented in Tabs. 8 and 9 for annual exceedance probabilities $q = 10^{-2}$ and $q = 10^{-4}$ respectively. Comparing these results to the exact long-term extreme response r_q in Tabs. 4 and 5, we observe that all the considered choices of p give reasonable rough estimates for the long-term response.

Table 4: The characteristic extreme response values as calculated by the different methods for an annual exceedance probability $q = 10^{-2}$.

	Approximate formulation			Exact formulation				
					r_q^{S} [cm]			
	$\tilde{r}_q^{\mathrm{F}}$ [cm]	$\tilde{r}_q^{\mathrm{S}}$ [cm]	$\tilde{r}_q$ [cm]	r_q^{F} [cm]	$C = 1$	$C = 10^4$	$C = 10^6$	r_q [cm]
EM1	56.4	48.7	54.4	56.8	49.6	58.7	58.5	61.8
EM2	2.52	2.39	2.42	2.54	2.42	2.55	2.55	2.58
EM3	53.3	49.7	51.6	53.7	50.6	61.0	60.8	62.1
EM4	246.8	243.4	243.4	249.2	248.3	284.9	284.6	284.6

Table 5: The characteristic extreme response values as calculated by the different methods for an annual exceedance probability $q = 10^{-4}$.

	Approximate formulation			Exact formulation				
					r_q^{S} [cm]			
	$\tilde{r}_q^{\mathrm{F}}$ [cm]	$\tilde{r}_q^{\mathrm{S}}$ [cm]	$\tilde{r}_q$ [cm]	r_q^{F} [cm]	$C = 1$	$C = 10^4$	$C = 10^6$	r_q [cm]
EM1	97.0	83.5	85.2	97.7	85.2	92.8	92.4	92.6
EM2	3.47	3.30	3.33	3.47	3.33	3.39	3.39	3.41
EM3	97.0	87.5	87.8	97.8	89.1	96.8	96.7	97.2
EM4	406.3	398.5	398.0	408.2	403.9	420.3	420.1	420.1

Table 6: The number of short-term response calculations performed for each of the long-term extreme response estimates in Tab. 4.

	Approximate formulation			Exact formulation				
					$n_{\mathrm{st}}^{\mathrm{S}}$			
	$\tilde{n}_{\mathrm{st}}^{\mathrm{F}}$	$\tilde{n}_{\mathrm{st}}^{\mathrm{S}}$	$\tilde{n}_{\mathrm{st}}$	$n_{\mathrm{st}}^{\mathrm{F}}$	$C = 1$	$C = 10^4$	$C = 10^6$	n_{st}
EM1	19	87	399960	23	111	111	113	399960
EM2	43	81	8040	43	81	71	67	8040
EM3	61	113	78993	60	117	225	147	78993
EM4	33	67	78993	33	67	81	177	78993

Table 7: The number of short-term response calculations performed for each of the long-term extreme response estimates in Tab. 5.

	Approximate formulation			Exact formulation				
					$n_{\mathrm{st}}^{\mathrm{S}}$			
	$\tilde{n}_{\mathrm{st}}^{\mathrm{F}}$	$\tilde{n}_{\mathrm{st}}^{\mathrm{S}}$	$\tilde{n}_{\mathrm{st}}$	$n_{\mathrm{st}}^{\mathrm{F}}$	$C = 1$	$C = 10^4$	$C = 10^6$	n_{st}
EM1	13	104	399960	18	110	109	126	399960
EM2	57	95	8040	57	94	89	85	8040
EM3	160	276	78993	256	384	167	155	78993
EM4	101	159	78993	105	151	82	190	78993

Table 8: The characteristic extreme response values as calculated by the environmental contour method using different quantile levels p for an annual exceedance probability $q = 10^{-2}$. The corresponding design points are illustrated by diamond markers in Figs. 12 and 13.

	r_q^p [cm]			
	$p = 0.80$	$p = 0.85$	$p = 0.90$	$p = 0.95$
EM1	58.6	59.6	61.0	63.3
EM2	2.60	2.64	2.69	2.79
EM3	55.3	56.2	57.6	59.7
EM4	258.5	263.3	269.7	280.1

Table 9: The characteristic extreme response values as calculated by the environmental contour method using different quantile levels p for an annual exceedance probability $q = 10^{-4}$. The corresponding design points are illustrated by diamond markers in Figs. 12 and 13.

	r_q^p [cm]			
	$p = 0.80$	$p = 0.85$	$p = 0.90$	$p = 0.95$
EM1	101.0	102.9	105.4	109.5
EM2	3.50	3.56	3.63	3.76
EM3	100.9	102.8	105.4	109.5
EM4	418.1	425.9	436.5	453.4

The exact fractile levels corresponding to the full long-term estimates can also be calculated. For the exact extreme response value r_q, the corresponding fractile level is given as

$$p_q = F_{\tilde{R}|\boldsymbol{W}}(r_q|\hat{\boldsymbol{w}}).$$

Table 10 shows the fractile levels corresponding to the exact extreme response values r_q in Tabs. 4 and 5. We see that there is a large variation in the obtained fractiles, indicating that one single fractile level does not give accurate estimates for all the considered cases. However, as seen in Tabs. 8 and 9, rough estimates can still be obtained. When regarded as rough approximations, Tabs. 8 and 9 show that the extreme response estimates are generally not overly sensitive to changing fractile levels. Still, if the fractile level should be much larger than 0.9, which is the case for EM3 and EM4 when $q = 10^{-2}$, the environmental contour method may underestimate the extreme response quite severely.

Considering Tabs. 8–10, reasonable choices for the fractile values are perhaps $p = 0.95$ for $q = 10^{-2}$ and $p = 0.80$ for $q = 10^{-4}$. Thus, p has a larger value for the highest annual exceedance probability. This is in contrast to the choices of $p = 0.90$ for $q = 10^{-2}$ and $p = 0.95$ for $q = 10^{-4}$, which are common for offshore structures [3]. It should also be noted that instead of using r_q, which is obtained by full numerical integration, the IFORM and ISORM estimates can be used to determine appropriate values for the fractile levels.

Table 10: The fractile levels p_q corresponding to the exact extreme response values r_q in Tabs. 4 and 5.

	EM1	EM2	EM3	EM4
p_q, $q = 10^{-2}$	0.92	0.77	0.98	0.96
p_q, $q = 10^{-4}$	0.43	0.69	0.66	0.81

5.3. Design points

In addition to giving an estimate for the characteristic extreme response, the inverse reliability methods will produce a design point which represents the most critical combination of environmental parameters for the specified annual exceedance probability q. The design point corresponding to the ISORM estimate r_q^{S} ($C = 10^6$) is shown in Fig. 12 for EM1. In Fig. 13 the design points are shown for the two-dimensional environmental models EM2, EM3 and EM4, also including the IFORM design points corresponding to the estimates r_q^{F} ($C = 1$). In addition, the contour method design points are shown in Figs. 12 and 13. As explained in Section 4.5, these have been obtained by maximizing the median value of the short-term CDF $F_{\tilde{R}|\boldsymbol{W}}(r|\boldsymbol{w})$ on the respective contours.

The relative contribution of different sea states to the long-term integral in Eqn. (4) is illustrated in Figs. 12 and 13 by the function $g(\boldsymbol{w})$. This function is defined as a normalized version of the integrand in Eqn. (4) for $r = r_q$. Specifically,

$$g(\boldsymbol{w}) = -\frac{1}{M} \ln\left(F_{\tilde{R}|\boldsymbol{W}}(r_q|\boldsymbol{w})\right) f_{\boldsymbol{W}}(\boldsymbol{w}),$$

where M is chosen such that the maximal value of $g(\boldsymbol{w})$ equals unity.

By considering Figs. 12 and 13, we observe that the main contribution to the long-term integral is located within a rather concentrated region. Furthermore, the design points quite successfully locate this region. The ISORM design point ($C = 10^6$) almost exactly pinpoints the location of the largest contribution. However, local maxima other than the main contribution might occur. This can be observed in the left part of Fig. 12, corresponding to $q = 10^2$ for EM1. If such a local maximum represent a significant contribution, this may result in an underestimation of the long-term extreme response as seen in the first row of Tab. 4. This is a known shortcoming of the inverse reliability methods, and they should therefore be used with some caution.

6. Concluding remarks

A framework for full long-term extreme response analysis has been demonstrated for a long-span case study bridge. Using recently developed IFORM and ISORM approaches, the extreme response was calculated in an efficient manner. Comparison with full numerical integration revealed that especially the ISORM method gives high accuracy. It has thus been shown that the proposed framework can be applied successfully for complex structures. Still, limitations

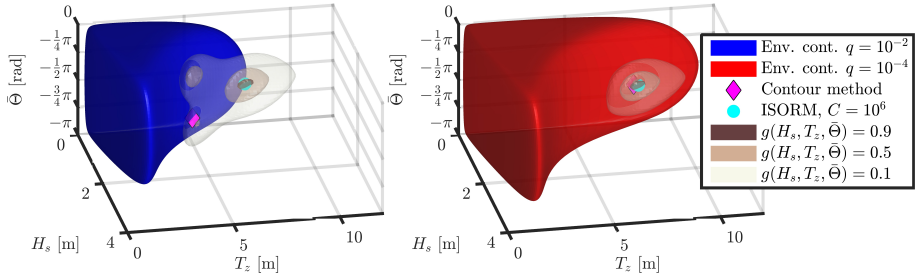

Figure 12: The design points corresponding to the characteristic extreme response value r_q^{S} (ISORM, $C = 10^6$) and the environmental contour method for annual exceedance probabilities $q = 10^{-2}$ (left) and $q = 10^{-4}$ (right). The contribution $g(\boldsymbol{w})$ to the long-term integral is also illustrated by displaying isosurfaces for the values 0.9, 0.5 and 0.1.

do exist, e.g. in the presence of multiple local maxima for the contribution to the long-term integral. Therefore, future work should focus on comparison with alternative approaches and further verification of the IFORM and ISORM methods, especially for nonlinear response.

The full long-term analysis was also compared with the environmental contour method. The results show that the contour method can be used to obtain rough estimates of the long-term extreme response. Furthermore, a proper fractile level p could be determined by comparison with the IFORM and ISORM results.

Acknowledgements

The authors are grateful for grants which are provided by Multiconsult ASA and the Research Council of Norway.

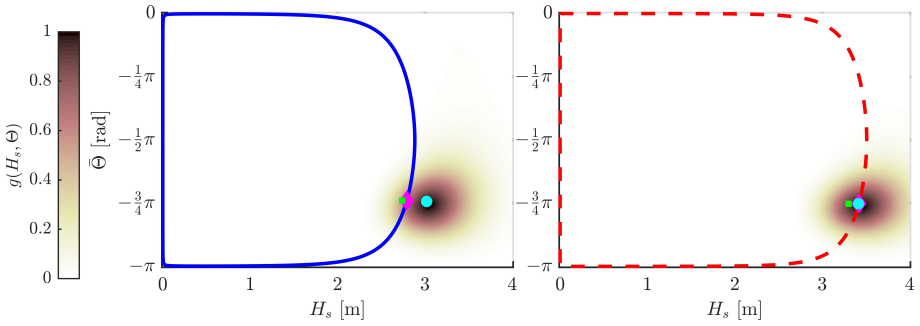

(a) EM2

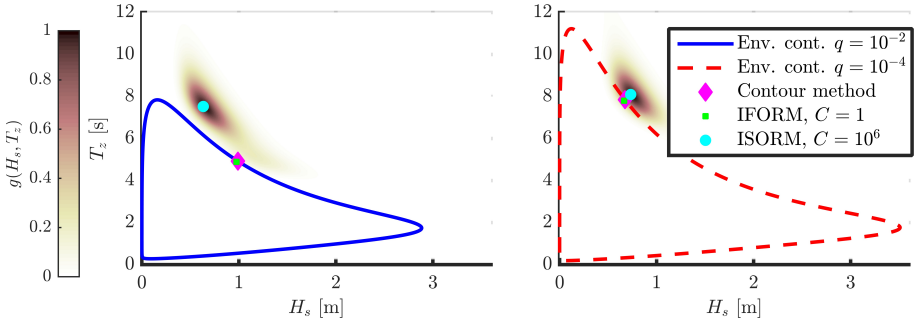

(b) EM3

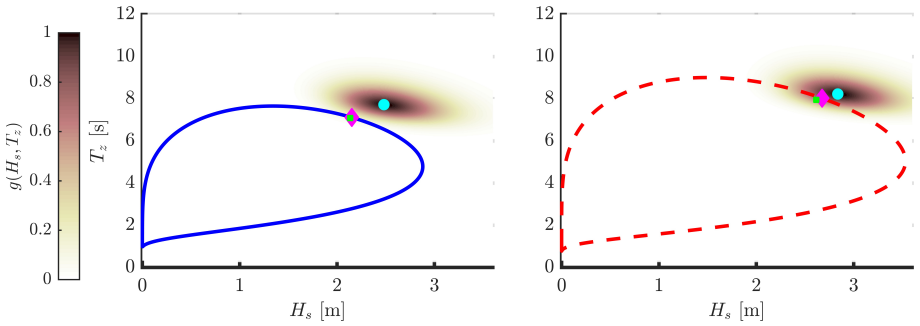

(c) EM4

Figure 13: The design points corresponding to the characteristic extreme response values r_q^{F} (IFORM, $C = 1$), r_q^{S} (ISORM, $C = 10^6$) and the environmental contour method for annual exceedance probabilities $q = 10^{-2}$ (left) and $q = 10^{-4}$ (right). The contribution $g(\boldsymbol{w})$ to the long-term integral is also illustrated in each case.

References

[1] Naess A, Moan T. Stochastic dynamics of marine structures. Cambridge: Cambridge University Press; 2012. ISBN 9781139021364. URL: http://ebooks.cambridge.org/ebook.jsf?bid=CBO9781139021364. doi:10.1017/CBO9781139021364.

[2] Haver S, Kleiven G. Environmental contour lines for design purposes: why and when? ASME Conf Proc 2004;2004(37432):337–45. URL: http://proceedings.asmedigitalcollection.asme.org/proceeding.aspx?articleid=1628932. doi:10.1115/OMAE2004-51157.

[3] Haver S, Winterstein S. Environmental contour lines: a method for estimating long term extremes by a short term analysis. Trans Soc Nav Archit Mar Eng 2010;116(October):116–27. URL: http://www.sname.org/HigherLogic/System/DownloadDocumentFile.ashx?DocumentFileKey=ccb5aac7-6b77-420b-b233-836fc6e13597.

[4] Winterstein SR, Ude TC, Cornell CA, Bjerager P, Haver S. Environmental parameters for extreme response: inverse FORM with omission factors. In: Proc. 6th Int. Conf. Struct. Saf. Reliab. Innsbruck, Austria; 1993,URL: http://www.rms-group.org/RMS_Papers/pdf/Todd/innsbruck.pdf.

[5] Huseby AB, Vanem E, Natvig B. A new approach to environmental contours for ocean engineering applications based on direct Monte Carlo simulations. Ocean Eng 2013;60:124–35. URL: http://www.sciencedirect.com/science/article/pii/S0029801812004532. doi:10.1016/j.oceaneng.2012.12.034.

[6] Huseby AB, Vanem E, Natvig B. Alternative environmental contours for structural reliability analysis. Struct Saf 2015;54:32–45. URL: http://linkinghub.elsevier.com/retrieve/pii/S0167473014001143. doi:10.1016/j.strusafe.2014.12.003.

[7] Montes-Iturrizaga R, Heredia-Zavoni E. Environmental contours using copulas. Appl Ocean Res 2015;52:125–39. URL: http://www.sciencedirect.com/science/article/pii/S0141118715000747. doi:10.1016/j.apor.2015.05.007.

[8] Agarwal P, Manuel L. Simulation of offshore wind turbine response for long-term extreme load prediction. Eng Struct 2009;31(10):2236–46. URL: http://dx.doi.org/10.1016/j.engstruct.2009.04.002. doi:10.1016/j.engstruct.2009.04.002.

[9] Li Q, Gao Z, Moan T. Modified environmental contour method for predicting long-term extreme responses of bottom-fixed offshore wind turbines. Mar Struct 2016;48:15–32. URL: http://www.sciencedirect.com/science/article/pii/S0951833916300181. doi:10.1016/j.marstruc.2016.03.003.

[10] Zhang Y, Beer M, Quek ST. Long-term performance assessment and design of offshore structures. Comput Struct 2015;154:101–15. URL: http://www.sciencedirect.com/science/article/pii/S004579491500067X. doi:10.1016/j.compstruc.2015.02.029.

[11] Sagrilo L, Naess A, Doria A. On the long-term response of marine structures. Appl Ocean Res 2011;33(3):208–14. URL: http://www.sciencedirect.com/science/article/pii/S0141118711000204. doi:10.1016/j.apor.2011.02.005.

[12] Giske FIG, Leira BJ, Øiseth O. Full long-term extreme response analysis of marine structures using inverse FORM. Probabilistic Eng Mech 2017;50:1–8. doi:10.1016/j.probengmech.2017.10.007.

[13] Giske FIG, Leira BJ, Øiseth O. Long-term extreme response analysis of marine structures using inverse SORM. In: ASME 2017 36th Int. Conf. Ocean. Offshore Arct. Eng.; vol. 3A. ASME. ISBN 978-0-7918-5765-6; 2017,URL: http://proceedings.asmedigitalcollection.asme.org/proceeding.aspx?doi=10.1115/OMAE2017-61409. doi:10.1115/OMAE2017-61409.

[14] Au SK, Beck JL. First excursion probabilities for linear systems by very efficient importance sampling. Probabilistic Eng Mech 2001;16(3):193–207. doi:10.1016/S0266-8920(01)00002-9.

[15] Papaioannou I, Papadimitriou C, Straub D. Sequential importance sampling for structural reliability analysis. Struct Saf 2016;62:66–75. URL: http://www.sciencedirect.com/science/article/pii/S0167473016300169. doi:10.1016/j.strusafe.2016.06.002.

[16] Au SK, Beck JL. Estimation of small failure probabilities in high dimensions by subset simulation. Probabilistic Eng Mech 2001;16(4):263–77. doi:10.1016/S0266-8920(01)00019-4.

[17] Ching J, Beck JL, Au SK. Hybrid Subset Simulation method for reliability estimation of dynamical systems subject to stochastic excitation. Probabilistic Eng Mech 2005;20(3):199–214. doi:10.1016/j.probengmech.2004.09.001.

[18] Dubourg V, Sudret B, Bourinet JM. Reliability-based design optimization using kriging surrogates and subset simulation. Struct Multidiscip Optim 2011;44(5):673–90. URL: http://link.springer.com/10.1007/s00158-011-0653-8. doi:10.1007/s00158-011-0653-8.

[19] Giske FIG, Leira BJ, Øiseth O. Efficient computation of cross-spectral densities in the stochastic modelling of waves and wave loads. Appl Ocean Res 2017;62:70–88. doi:10.1016/j.apor.2016.11.007.

[20] Giske FIG, Leira BJ, Øiseth O. Stochastic Modelling of Wave Loads on Floating Bridges : Efficient Calculation of Cross-Spectral Densities. In:

19th Congr. IABSE, Challenges Des. Constr. an Innov. Sustain. Built Environ. September. ISBN 978-3-85748-144-4; 2016, p. 48–56.

[21] Hauser D, Kahma K, Krogstad H. Measuring and analysing the directional spectra of ocean waves. Luxembourg: Publications Office of the European Union; 2005. ISBN 92-898-0003-8.

[22] Stansberg CT, Contento G, Hong SW, Irani M, Ishida S, Mercier R, et al. The specialist committee on waves final report and recommendations to the 23rd ITTC. In: Proceedings of the 23rd ITTC. 2002, p. 505–736. URL: http://ittc.info/media/1469/waves.pdf.

[23] DNV . Wadam. 2014. Høvik, Norway.

[24] Sigbjörnsson R. Stochastic theory of wave loading processes. Eng Struct 1979;1(2):58–64. URL: http://www.sciencedirect.com/science/article/pii/0141029679900142. doi:10.1016/0141-0296(79)90014-2.

[25] Langen I, Sigbjörnsson R. On stochastic dynamics of floating bridges. Eng Struct 1980;2(4):209–16. URL: http://www.sciencedirect.com/science/article/pii/0141029680900024. doi:10.1016/0141-0296(80)90002-4.

[26] Ochi MK. Applied probability and stochastic processes in engineering and physical sciences. New York: Wiley; 1990. ISBN 0471857424. URL: http://books.google.com/books?ei=JFOBU7TtFYHcObC4gLgK{&}id=ID3xAAAAMAAJ{&}pgis=1.

[27] Kvåle KA, Sigbjörnsson R, Øiseth O. Modelling the stochastic dynamic behaviour of a pontoon bridge: A case study. Comput Struct 2016;165:123–35. URL: http://www.sciencedirect.com/science/article/pii/S004579491500334X. doi:10.1016/j.compstruc.2015.12.009.

[28] Dassault Systèmes Simulia Corp. . Abaqus. 2014. Providence, Rhode Island, USA.

[29] Naess A. Technical note: On the long-term statistics of extremes. Appl Ocean Res 1984;6(4):227–8. URL: http://www.sciencedirect.com/science/article/pii/0141118784900610. doi:10.1016/0141-1187(84)90061-0.

[30] Melchers RE. Structural reliability analysis and prediction. 2nd ed.; John Wiley & Sons; 1999. ISBN 9780471987710.

[31] Giske FIG, Leira BJ, Øiseth O. Long-term stochastic extreme response analysis of floating bridges. Procedia Eng 2017;199:1175–80. URL: http://www.sciencedirect.com/science/article/pii/S1877705817337888. doi:10.1016/j.proeng.2017.09.305.

[32] DNV . DNV-RP-C205 Environmental conditions and environmental loads. Tech. Rep. October; DNV; Høvik, Norway; 2010. URL: https://rules.dnvgl.com/docs/pdf/DNV/codes/docs/2010-10/RP-C205.pdf.

[33] Bitner-Gregersen EM, Haver S. Joint environmental model for reliability calculations. In: Proc. First Int. Offshore Polar Eng. Conf. Edinburgh, United Kingdom: International Society of Offshore and Polar Engineers; 1991, p. 246–53. URL: https://www.onepetro.org/conference-paper/ISOPE-I-91-031.